AIAA JOURNAL
Vol. 46, No. 4, April 2008

Flutter of Partially Rigid Cantilevered Two-Dimensional Plates in Axial Flow

Roeland De Breuker,* Mostafa M. Abdalla,† and Zafer Gürdal‡
Delft University of Technology, 2629 HS Delft, The Netherlands

DOI: 10.2514/1.31887

The introduction of adaptive materials for active camber line shape control favors flexible wing designs, thus making adaptive wings more susceptible to instability phenomena. Motivated by a new wing concept for micro aerial vehicle applications, the aeroelastic stability of partially rigid cantilevered plates in an axial flow is investigated. The plate is modeled as a beam having a rigid and a flexible part. The beam is modeled using the classical Euler–Bernoulli bending theory, the unsteady aerodynamic pressure is modeled using Theodorsen's theory, and the Rayleigh–Ritz method is used to obtain a discrete model. Stability analysis is carried out in Laplace's domain. The results indicate that a partially rigid cantilevered plate in an axial flow does not show static aeroelastic divergence but exhibits dynamic aeroelastic instability. The flutter velocity at which this instability occurs is dependent on the ratio of the flexible length to the total length of the plate and the mass ratio. Adding a rigid part ahead of a flexible plate can have a stabilizing or destabilizing effect on the aeroelastic behavior of the flexible plate, depending on the mass ratio. The phase-angle difference between the upstream and downstream part of the two-dimensional plate is shown to be dependent on the mass ratio and flexible length fraction. Jumps in the flutter diagram occur because of changes in flutter mode, and the flexible length fraction also affects these jump phenomena. The jumps are shown to be the result of eigenvalue branch collision. There are multiple critical flow conditions for mass ratios around the jumps. Therefore, a new practical flutter boundary definition is introduced to remove the overlap between flutter modes near the jumps. The flutter diagram calculated according to the new definition shows better agreement with published time domain simulations.

Nomenclature

$\mathbf{A}$	=	aerodynamic matrix
A_i	=	Fourier coefficient
b	=	half-chord
$C(\bar{s})$	=	Theodorsen's function
D	=	plate bending stiffness
$\boldsymbol{F}$	=	force vector
f	=	ratio of the flexible plate length to the total plate length
G	=	decay factor
H_n	=	Hankel function of the nth kind
$\mathbf{K}$	=	stiffness matrix
K_n	=	modified Bessel function of the second kind
k	=	reduced frequency
L	=	length of the flexible plate
M	=	bending moment
$\mathbf{M}$	=	mass matrix
m	=	structural mass
n	=	number of modes
p	=	pressure
q	=	dynamic pressure
$\boldsymbol{q}$	=	degree-of-freedom vector
s	=	Laplace variable
$\bar{s}$	=	nondimensional Laplace variable
$\mathcal{T}$	=	kinetic energy
U	=	undisturbed flow velocity
$\tilde{U}$	=	nondimensional airspeed
$\mathcal{U}$	=	potential energy
$\boldsymbol{v}$	=	generalized momentum vector
w	=	out-of-plane displacement
γ	=	vorticity per unit length
δ	=	reduced damping
θ	=	transformed coordinate
ρ	=	air density
$\tilde{\rho}$	=	mass ratio of the air mass to the flexible plate mass
σ	=	damping
ϕ	=	velocity potential
φ	=	phase angle
ψ	=	shape function
ω	=	frequency

Subscripts

a	=	aerodynamic
c	=	circulatory
nc	=	noncirculatory
s	=	structural

Superscripts

$\hat{}$	=	Laplace transform
$\dot{}$	=	first time derivative
$\ddot{}$	=	second time derivative

Presented as Paper 1730 at the 47th AIAA/ASME/ASCE/AHS/ASC Structures, Structural Dynamics, and Materials Conference, Newport, RI, 1–4 May 2006; received 1 May 2007; revision received 27 November 2007; accepted for publication 30 November 2007.

*Ph.D. Student, Faculty of Aerospace Engineering, Aerospace Structures Group, Kluyverweg 1. AIAA Student Member.

†Assistant Professor, Faculty of Aerospace Engineering, Aerospace Structures Group, Kluyverweg 1. AIAA Member.

‡Chair of Aerospace Structures, Faculty of Aerospace Engineering, Aerospace Structures Group, Kluyverweg 1. AIAA Associate Fellow.

I. Introduction

THE introduction of new adaptive materials for structural applications creates the potential of distributed actuation of structures. Adaptive materials can be used to actively deform structures to achieve multiple functions. By changing its shape, the wing surface can potentially fulfill the additional role of a control surface, eliminating the need for mechanical parts, leading to a less complex structure and potential weight savings. Moreover, by

morphing a wing in a smooth fashion, the aerodynamic drag may be reduced. If the structure is stiff, the energy required for the deformation will be large, therefore, a flexible construction, permitting deformations at reasonable energy cost, is indispensable. Because of this increased flexibility, morphing structures are expected to be more sensitive to instabilities resulting from interaction with fluid flow over the structure.

Practical applications of morphing structures are currently a subject of intensive research [1]. Both aircraft configuration morphing as well as airfoil morphing are currently under study. The latter investigation also includes the application of adaptive materials. Morphing airfoils can be adapted optimally to any given flight condition. Different scenarios for these adaptations have been studied by Gano and Renaud [2], and Joshi et al. [3]. Research has been carried out at the Delft University of Technology, The Netherlands, on the development of an adaptive wing capable of morphing part of its camber line for micro aerial vehicle (MAV) application [4–8]. The adaptive wing concept, which is referred to as the Delft wing, consists of a flexible flat plate attached to a stiff leading edge. This leading edge has a significantly larger stiffness than the plate and provides the necessary torsional and bending stiffness of the wing. Therefore, the main emphasis of the investigation is on the stability of the flexible plate in double-sided axial flow rather than classical bending-torsion flutter.

Stability of plates with various boundary conditions subjected to one- or two-sided flow have been studied extensively in literature. Thorough research was carried out by Dowell in the sixties [9,10]. Unlike classical plate flutter, which assumes supersonic flow, Dowell's investigation assumes unsteady potential flow and structural nonlinearities. An overview of aeroelasticity of plates and shells is given in the monograph by Dowell [11]. Kornecki et al. [12] and Guo and Païdoussis [13] also studied plates subjected to a subsonic axial flow having various boundary conditions. Cantilevered plates in axial flow in particular have also been a topic of interest. An extensive discussion on cantilevered plates in axial flow is given in the book by Païdoussis [14]. The aeroelastic instabilities of cantilevered plates in axial flow show remarkable similarities to the behavior of cantilevered pipes conveying fluids. They are also susceptible to flutter oscillations in modes similar to those of fluttering cantilevered plates, and they also exhibit jump phenomena in their flutter boundary diagram. This has been shown and covered extensively in literature [15–18].

Two-dimensional cantilevered plates are investigated by Shayo [19], which is an extension of the work of Kornecki et al. [12]. Nonlinear effects and limit cycle oscillations of a fluttering plate were also considered by Weiliang and Dowell [20], Tang and Dowell [21], Attar et al. [22], and Tang and Païdoussis [23,24]. Tang et al. [25] also investigated two-dimensional plates in a three-dimensional flow, and verified the obtained numerical results with experiments.

The aforementioned researchers all assume inviscid flow. However, research has also been carried out to investigate the effect of viscosity on the aeroelastic stability of cantilevered plates in axial flow by Watanabe et al. [26] and Balint and Lucey [27], who demonstrated that viscous effects do not change the flutter behavior qualitatively.

Cantilevered strips have been studied by Yadykin et al. [28] who take into account both structural and aerodynamic nonlinearities. Paper flutter has been investigated by Watanabe et al., both theoretically [26] and experimentally [29]. The biomechanical problem of human snoring has been addressed by Huang [30], Tanida [31], and Balint and Lucey [27]. These authors assumed that the origin of snoring by humans was caused by palatal flutter, and modeled the soft palate as a flexible cantilevered plate in an axial flow.

Although the phenomenon of flutter of cantilevered plates is well known, the onset mechanism still remains somewhat obscure. Shayo [19] studied the effect of the wake on the aeroelastic stability of such a plate. He concluded that wake effects are more important for longer plates. Huang [30] demonstrated that quasi-steady aerodynamics and circulatory (wake-related) effects are responsible for the onset of flutter. Watanabe et al. [26] showed that the coupling between natural modes is responsible for the onset of cantilevered plate flutter. Argentina and Mahadevan [32] especially focused on the discrepancy between theory and experiments, and concluded that an accurate prediction of the onset of flutter cannot be carried out without taking certain nonlinearities into account. Tang and Païdoussis [24] investigated the effect of the wake on the flutter behavior and found that the wake has a larger influence on the stability of short plates than on long plates.

Partially rigid cantilevered plates in axial flow have also been subject of research. The first to take into account the effect of a hard plate on a soft plate were Tanida [31], Tang and Dowell [21], and Tang et al. [25]. The work by Tanida [31] was based on a simplified model and certain assumptions regarding the phase difference along the plate. As will be shown later in this paper, these phase-difference assumptions appear not to be valid for all circumstances. The latter two papers took the effect of a rigid part into account but did not study the effect of the rigid part in detail. No results, to the best of the authors' knowledge, of the parametric variation of flutter speed vs the flexible part fraction exist in literature, apart from De Breuker et al. [7] and, more recently, by Tang and Païdoussis [23]. The current paper extends the two previously mentioned papers by investigating the complete range of flexible part fractions and their influence on flutter speed, phase difference along the plate, and the divergence speed. Furthermore, the well-known phenomenon of mode jumping is addressed in more detail, and root locus plots are used to give a possible explanation for the discrepancies between analytic and experimental results.

In the present paper, the problem of flutter of partially rigid cantilevered plates in double sided incompressible flow is considered in the Laplace domain. Using linear analysis, eigenvalues and eigenmodes at the initial stages of flutter can be extracted, which provides physical insight into the modal phenomena involved. The effect of adding a rigid part, varying from zero length to the entire chord, on the aeroelastic stability of the flexible part is studied. The main emphasis of the results is to demonstrate how the flutter properties and phase-angle distribution of the partially rigid cantilevered plate depend on the ratio of the plate mass to the air mass, and the ratio between the flexible part of the plate to its entire length. Root locus plots showing the variation of aeroelastic system eigenvalues with speed are used to study the flutter mode behavior.

The remainder of this paper is arranged as follows. Section II describes the problem at hand and an idealized model of the Delft wing is presented. In Sec. III, the aerodynamic model, based on Theodorsen's theory, is given. Section IV presents the structural model of the plate, where a discrete model is obtained using the Rayleigh–Ritz technique. Section V contains the flutter analysis, formulated in the Laplace domain, based on an eigenvalue analysis. In Sec. VI, the results from the analysis are compared with published results in literature. Section VII presents the results and a discussion is given. In Sec. VIII, pertinent conclusions are drawn.

II. Problem Description

Current research at the Delft University of Technology, The Netherlands, involves the design of an adaptive wing for micro aerial vehicle applications. A schematic drawing of such a wing is shown in Fig. 1, and a wing prototype for the MAV is displayed in Fig. 2.

The wing consists of a stiff leading edge made of an aluminium skin with foam core which is attached to the MAV fuselage. To this leading edge, a highly flexible plate is attached, again made of aluminium. The plate is activated using piezoelectric (PZT) patches glued to the aluminium surface on either side in a bimorph configuration. When a voltage is applied to the PZT patches, the plate bends, changing lift. This way, the wing can be operated without the need for control surfaces, which reduces complexity and weight.

Because of the nature and intended goal of the investigation, simplified models can be employed for both the structure and the fluid. The plate is idealized as a cantilevered beam, oriented in chordwise direction, of length $2b$, part of which is rigid (representing the stiff leading-edge portion) and the remaining part of length L is flexible (representing the chordwise bending of the plate) as indicated in Fig. 3. Modeling a two-dimensional plate as a beam

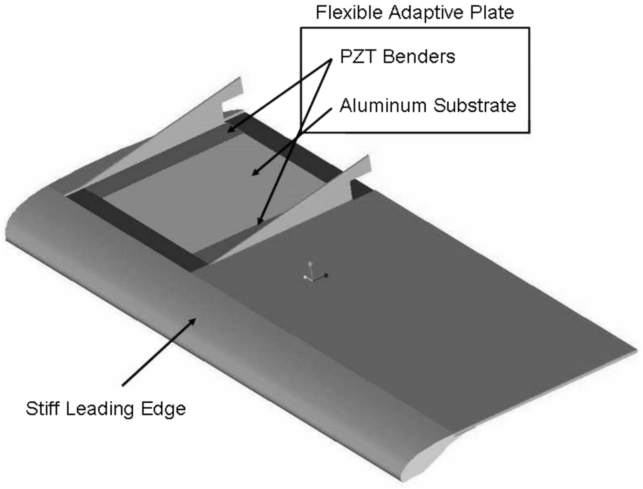

Fig. 1 Concept layout of an adaptive wing.

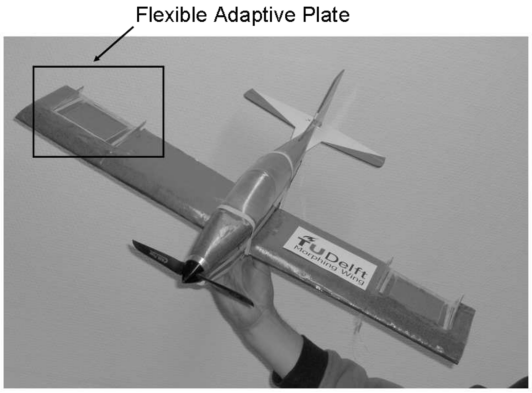

Fig. 2 Adaptive wing with flexible plate on a remote-controlled aircraft.

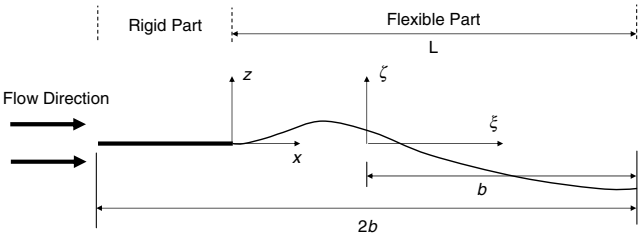

Fig. 3 Idealized adaptive wing.

gives similar results for length-to-width ratios up to two, as shown by Dowell [9].

Both the fluid and the structure are modeled using a semi-analytical approach. The structure is discretized using the Rayleigh–Ritz technique, which has been proven to provide good results, even for nonlinear aeroelastic cantilevered plate problems [20]. Because only the initial stages of flutter are of interest, exhibiting only small oscillations, linear kinematic assumptions [33] are adopted for the strain-displacement relation. The aerodynamic model is based on Theodorsen's theory [34]. Special care is given to the treatment of the rigid part of the airfoil in generating the aerodynamic matrices.

III. Structural Model

The wing is modeled using a linear Euler–Bernoulli beam [33]. The unknown *out-of-plane* displacement w is approximated by means of the Rayleigh–Ritz assumed modes method. The solution is represented with a series of assumed modes ψ^s for the flexible part of the airfoil (Fig. 3), which is dependent on the spatial coordinate x, measured from the intersection between the rigid and flexible part:

$$w(x,t) = q_i(t)\psi_i^s(x) \tag{1}$$

where q_i are the modal amplitudes. The mode shapes are expressed as polynomials that satisfy the essential boundary conditions at the root. The polynomials used in this paper are orthonormal [35]. The use of orthonormal shape functions is not a requirement of the Rayleigh–Ritz method, but their use prevents ill-conditioning of the structural and aerodynamic matrices.

The unknown vector of degrees of freedom $\boldsymbol{q}(t)$ is then determined using Hamilton's variational principle, neglecting structural damping:

$$\int_{t_1}^{t_2} \delta(\mathcal{T} - \mathcal{U})\,\mathrm{d}t - \int_{t_1}^{t_2}\int_0^L \Delta p\,\delta w\,\mathrm{d}x\,\mathrm{d}t = 0 \tag{2}$$

where Δp is the aerodynamic pressure, modeled in the next section. $\mathcal{T}$ and $\mathcal{U}$ are the kinetic and strain energy, respectively, which are given by

$$T = \frac{1}{2}\int_0^L m\dot{w}^2\,\mathrm{d}x \tag{3}$$

$$\mathcal{U} = \frac{1}{2}\int_0^L \left(M\frac{\mathrm{d}^2 w}{\mathrm{d}x^2}\right)\mathrm{d}x \tag{4}$$

where m is the mass per unit length of the flexible part of the plate and M the bending moment acting on the midsurface of the plate. A dot $\dot{(\,)}$ indicates the derivative with respect to time. After substitutions, the governing equation takes the following matrix form:

$$\mathbf{M}_s\ddot{\boldsymbol{q}} + \mathbf{K}_s\boldsymbol{q} = \boldsymbol{F}_a \tag{5}$$

where $\mathbf{M}_s$ is the mass matrix and $\mathbf{K}_s$ is the stiffness matrix. Subscript s indicates that the matrices are structural matrices. A double dot $\ddot{(\,)}$ indicates the second derivative with respect to time, and the aerodynamic loading $\boldsymbol{F}_a$ is expressed as

$$\boldsymbol{F}_a = \int_0^L \Delta p\boldsymbol{\psi}^s\,\mathrm{d}x \tag{6}$$

The structural mass matrix assumes the following form:

$$\mathbf{M}_s = mL\int_0^1 \boldsymbol{\psi}^s(\boldsymbol{\psi}^s)^T\,\mathrm{d}x = mL\mathbf{I} \tag{7}$$

where $\mathbf{I}$ is the identity matrix, which follows from the use of orthonormal shape functions. The structural stiffness matrix is given as

$$\mathbf{K}_s = \frac{D}{L^3}\int_0^1 \frac{\mathrm{d}^2\boldsymbol{\psi}^2}{\mathrm{d}x^2}\frac{\mathrm{d}^2(\boldsymbol{\psi}^s)^T}{\mathrm{d}x^2}\,\mathrm{d}x \tag{8}$$

where D is the plate bending stiffness.

IV. Aerodynamic Model

The origin of the aerodynamic coordinate system is located in the middle of the airfoil chord (see Fig. 3). The flow is modeled using incompressible, inviscid, irrotational assumptions, governed by the familiar Laplace equation [36] of the perturbation velocity potential ϕ. Here, a numerical approach to calculate the aerodynamic pressure on the plate is presented following Theodorsen's theory [34]. Closed-form solutions for the unsteady pressure on curved plates described by a cubic polynomial have been derived by Mesaric and Kosel [37]. According to Theodorsen [34], small oscillations are assumed and the following linearized boundary condition is enforced:

$$\frac{\partial \phi}{\partial \zeta} = \frac{\partial w}{\partial t} + U\frac{\partial w}{\partial \xi} \tag{9}$$

where U is the undisturbed flow velocity.

The airfoil wake has a strength (γ_w) with vortices being shed in a periodic fashion:

$$\gamma_w = \hat{\gamma} e^{st} \tag{10}$$

where $s = \sigma + i\omega$, σ is the damping, and ω is the frequency.

The pressure over the airfoil is split up into two parts, a circulatory (subscript c) part, associated with the wake, and a noncirculatory (subscript nc) part:

$$\Delta p = \Delta p_c + \Delta p_{\text{nc}} \tag{11}$$

The pressure difference can be obtained from the perturbation potential using the unsteady Bernoulli equation:

$$\Delta p = -2\rho\left(\frac{\partial \phi}{\partial t} + U\frac{\partial \phi}{\partial \xi}\right) \tag{12}$$

where ρ is the density of the surrounding air. The noncirculatory potential can be found by integrating the vorticity distribution over the length and by multiplying it with ρ and U:

$$\phi(\theta, t) = \rho U \int_0^{\pi} \gamma(\theta, t) \sin\theta \, \mathrm{d}\theta \tag{13}$$

The noncirculatory vortex distribution γ is expressed according to Glauert's series [38]:

$$\gamma(\theta, t) = 2U\left[A_0(t)\left(\frac{1+\cos\theta}{\sin\theta}\right) + \sum_{n=1}^{\infty} A_n(t)\sin n\theta\right] \tag{14}$$

where the Fourier coefficients $A_0 \ldots A_n$ are defined as

$$A_0 = \frac{1}{\pi}\int_0^{\pi} w(\theta, t)\, \mathrm{d}\theta \tag{15}$$

$$A_n = \frac{2}{\pi}\int_0^{\pi} w(\theta, t)\cos(n\theta)\, \mathrm{d}\theta \tag{16}$$

The variable θ is obtained by means of the transformation $\xi = b\cos\theta$.

The circulatory pressure is determined by enforcing the Kelvin circulation theorem and the Kutta condition as

$$\triangle p_c = -2\rho U\left(A_0(t) + \frac{A_1(t)}{2}\right)[C(\bar{s}) - 1]\left(\frac{1+\cos\theta}{\sin\theta}\right) \tag{17}$$

In this expression, $C(\bar{s})$ is Theodorsen's function:

$$C(\bar{s}) = \frac{H_1^{(2)}(\bar{s})}{H_1^{(2)}(\bar{s}) + iH_0^{(2)}(\bar{s})} \tag{18}$$

where expressions $H_n^{(2)}$ are nth-order Hankel functions of the second kind. The Laplace domain variable s is nondimensionalized to $\bar{s}$, using U and b, which is the half-chord

$$\bar{s} = \frac{b}{U}s = (\delta + ik) \tag{19}$$

in which δ is the reduced damping and k is the reduced frequency.

This form of Theodorsen's function is only valid for positive imaginary (or reduced frequency) numbers. Therefore, in the present investigation, the original expressions in terms of modified Bessel functions of the second kind are used to be able to cope with negative frequencies:

$$C(\bar{s}) = \frac{K_1(\bar{s})}{K_0(\bar{s}) + K_1(\bar{s})} \tag{20}$$

Next, the aerodynamic mode shapes $\psi^a(\xi)$ are discussed. These shapes are identical to the structural mode shapes $\psi^s(x)$ except that they also contain the rigid part of the airfoil.

$$\psi^a = \begin{cases} 0 & \text{for } -b \le \xi \le 2b(1-f) \\ \psi^s & \text{for } 2b(1-f) < \xi \le 2b \end{cases} \tag{21}$$

The flexible length fraction f is defined as

$$f = \frac{L}{2b} \tag{22}$$

with L being the length of the flexible part of the airfoil.

The components of the generalized aerodynamic force vector $\boldsymbol{F}_a$ are defined using Eq. (4), which means that the ith element of $\boldsymbol{F}_a$ is expressed as

$$F_{a,i} = \int_0^{\pi}\sum_{j=1}^{n} \triangle p_j \psi_i^a(\theta)\sin\theta \, \mathrm{d}\theta \tag{23}$$

where n is the number of modes.

The aerodynamic force vector $\mathbf{F}_a$ is defined as:

$$\boldsymbol{F}_a = -\frac{1}{2}\rho b^2 \mathbf{M}_a \ddot{\boldsymbol{q}} - \frac{1}{2}\rho U b \mathbf{C}_a(\bar{s})\dot{\boldsymbol{q}} - \frac{1}{2}\rho U^2 \mathbf{K}_a(\bar{s})\boldsymbol{q} \tag{24}$$

where matrices $\mathbf{M}_a$, $\mathbf{C}_a$, and $\mathbf{K}_a$ are the mass, damping, and stiffness matrix, respectively. Subscript a indicates that these matrices are aerodynamic matrices. Expression $\frac{1}{2}\rho U^2$ is the dynamic pressure q. The aerodynamic matrices are constructed for all flexible part fractions ranging from an almost rigid to a fully flexible plate using the symbolic manipulation software Mathematica.

V. Stability Analysis

In this section, aeroelastic analysis is conducted to determine both static and dynamic aeroelastic stability. First, static aeroelasticity will be investigated. The steady-state aeroelastic Eq. (5) reduces to

$$[\mathbf{K}_s + q\mathbf{K}_a(\bar{s})]\boldsymbol{q} = 0 \tag{25}$$

This is an eigenvalue problem for the dynamic pressure q. A positive real eigenvalue q indicates the divergence speed, whereas negative values show the absence of divergence.

Flutter analysis is conducted in Laplace's domain to determine the stability boundaries of the plate. At the stability boundary, the motion is harmonic and takes the form

$$\boldsymbol{q} = \hat{\boldsymbol{q}} e^{st} \tag{26}$$

where $\hat{\boldsymbol{q}}$ is the modal amplitude.

Substituting the nondimensional $\bar{s}$ [Eq. (19)] into the aeroelastic Eq. (5) yields the following equation:

$$\left[\left(\frac{U}{b}\right)^2 \bar{s}^2\left(\mathbf{M}_s + \frac{1}{2}\rho b^2 \mathbf{M}_a\right) + \frac{U}{b}\bar{s}\frac{1}{2}\rho U b \mathbf{C}_a(\bar{s}) + [\mathbf{K}_s + q\mathbf{K}_a(\bar{s})]\right]\hat{\boldsymbol{q}} = [\bar{s}^2\mathbf{M} + \bar{s}\mathbf{C}(\bar{s}) + \mathbf{K}(\bar{s})]\hat{\boldsymbol{q}} = \mathbf{0} \tag{27}$$

Equation (27) is a quadratic eigenvalue problem. To obtain the pole locations, the system is transformed into a standard eigenvalue problem with the introduction of the generalized momentum $\hat{\boldsymbol{v}} = \bar{s}\mathbf{M}\hat{\boldsymbol{q}}$. This yields the following matrix equation:

$$\bar{s}\begin{bmatrix}\hat{\boldsymbol{q}} \\ \hat{\boldsymbol{v}}\end{bmatrix} = \begin{bmatrix}\mathbf{0} & \mathbf{M}^{-1} \\ -\mathbf{K}(\bar{s}) & -\mathbf{C}(\bar{s})\mathbf{M}^{-1}\end{bmatrix}\begin{bmatrix}\hat{\boldsymbol{q}} \\ \hat{\boldsymbol{v}}\end{bmatrix} \tag{28}$$

which can be recast as

$$[\bar{s}\mathbf{I} - \mathbf{A}(\bar{s})]\hat{\boldsymbol{x}} = \mathbf{0} \tag{29}$$

where the vector $\hat{\boldsymbol{x}} = \{\hat{\boldsymbol{q}}, \hat{\boldsymbol{v}}\}^T$ is the vector containing the generalized coordinates and generalized momentum, and $\mathbf{A}(\bar{s})$ is the aeroelastic system operator. For the solution of the system $\bar{s}$, an initial guess is made by calculating the eigenfrequencies of the aeroelastic system when there is no flow velocity present. Using this value for $\bar{s}$, the eigenvalues of $\mathbf{A}(\bar{s})$ are calculated. The eigenvalue closest to the guess is selected and used as the new guess. This process is repeated until converged.

VI. Validation of the Results

To observe the difference between the expression of Theodorsen's function with modified Bessel function of the second kind [Eq. (20)] and Hankel functions [Eq. (18)], both expressions are plotted for positive and negative k in Fig. 4. For positive values of the reduced frequency, the well-known half-ellipse in the fourth quadrant of the complex plane is obtained for both Eqs. (18) and (20). For negative k though, the modified Bessel functions of the second kind give the mirrored image of the previously mentioned ellipse along the real axis. The original Theodorsen expression, however, diverges as can be concluded clearly from the graph.

To validate the results obtained, they are compared with results published in literature. Three nondimensional parameters are introduced following Huang [30] and adapted for partially rigid plates. The plate mass ratio is defined as

$$\tilde{\rho} = \frac{\rho b f}{m} \tag{30}$$

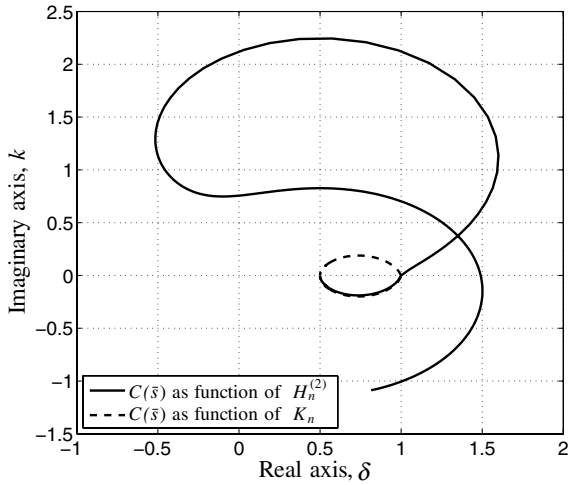

Fig. 4 Comparison between two expressions for Theodorsen's function for positive and negative frequencies.

The nondimensional speed $\tilde{U}$ is introduced as

$$\tilde{U} = \frac{U}{\omega_1 b f} \tag{31}$$

where ω_1 is the first bending frequency of the plate. The ratio of the vibration amplitude at one cycle to its value at the previous cycle, called the decay factor G, is defined as

$$G = e^{2\pi \frac{\delta}{\omega}} \tag{32}$$

The convergence of the flutter solution for increasing number of shape functions is investigated for several mass ratios from $\tilde{\rho} = 0$ to $\tilde{\rho} = 5$ and for a fully flexible plate ($f = 1$). The results are displayed in Fig. 5. A wide range of mass ratios from $\tilde{\rho} = 0$ to $\tilde{\rho} = 5$ is considered because, as it will appear later in the discussion of the results, the flutter mode shape is dependent on the mass ratio. It is concluded from Fig. 5 that eight shape functions will be sufficient for an acceptable level of accuracy for a wide range of mass ratios. It is assumed that a sufficient number of shape functions for the flutter solution also produces converged results for divergence calculations.

Results for damping, frequency, vibration amplitude decay, and phase-angle distribution are compared with numerical results obtained by Huang [30]. The nondimensional damping δ (Fig. 6a) and the frequency ratio ω/ω_1 (Fig. 6b) are compared for the case of a fully flexible plate ($f = 1.0$). The decay factor G and the phase-angle distribution φ are validated, as shown in Figs. 7a and 7b, respectively.

Good agreement with the time domain results from Huang [30] is obtained. The flutter boundary is also validated against results obtained by Guo and Païdoussis [13], Watanabe et al. [26], Tang and Païdoussis [24], and Huang [30], respectively. Good agreement is generally also observed as can be inspected in Fig. 8. The results of Huang [30] match the results of the model described in this paper exactly, making them barely visible in the graph. Interestingly enough, the graph plotted in Fig. 8 is qualitatively comparable to earlier published results for cantilevered slender pipes conveying fluid [15,16,18].

VII. Results and Discussion

It has already been shown extensively in the literature [11,12,14] that cantilevered plates do not show divergence. Here, it is investigated whether this also holds for partially rigid cantilevered plates. Static aeroelastic divergence is investigated for several mass ratios ($\tilde{\rho} \in [0.00 \ldots 5.00]$) and flexible part fractions ($f \in [0.1 \ldots 1.0]$). The results are given in Fig. 9. As can be observed, the eigenvalues are all negative over the investigated range. They remain negative, even for very large mass ratios. This concludes that a partially rigid cantilevered plate does not exhibit divergence.

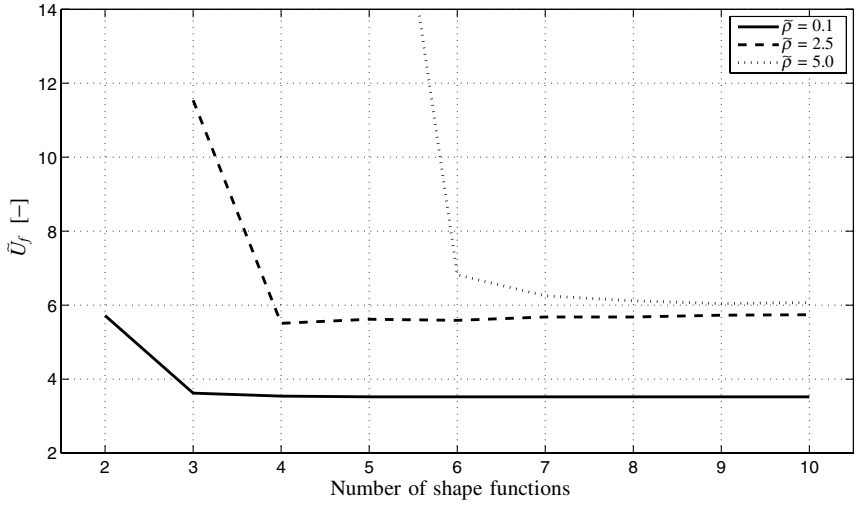

Fig. 5 Convergence of flutter speed with increasing number of shape functions for various mass ratios for fully flexible plate, $f = 1$.

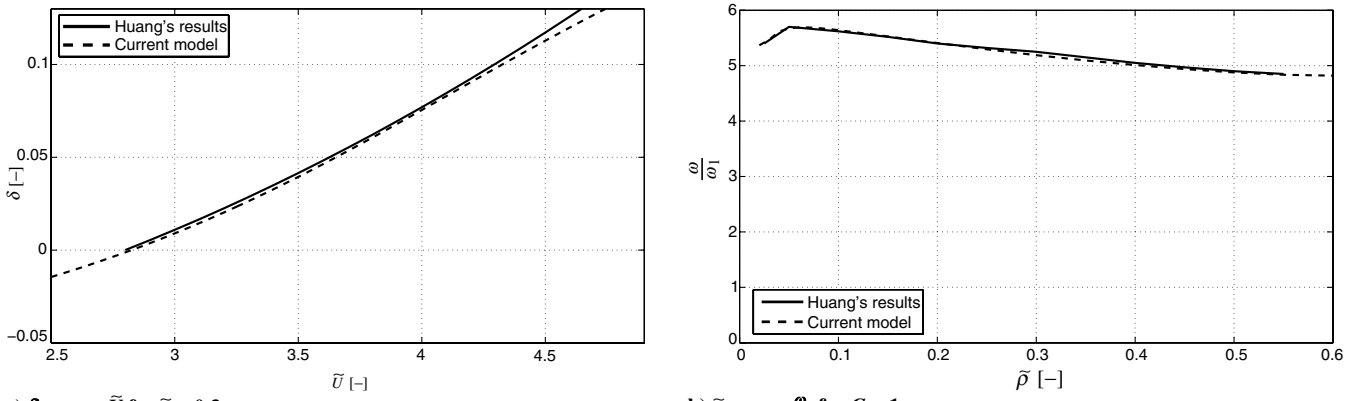

a) δ versus $\widetilde{U}$ for $\widetilde{\rho}$ = 0.3 **b) $\widetilde{\rho}$ versus $\frac{\omega}{\omega_1}$ for G = 1**

Fig. 6 Validation of oscillation damping and frequency with Huang's [30] results.

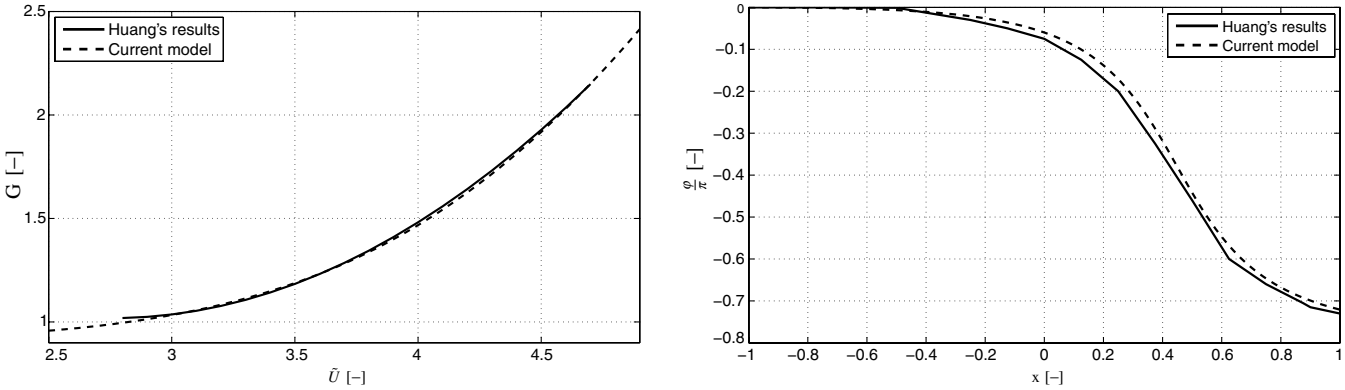

a) G Versus $\widetilde{U}$ for $\widetilde{\rho}$ = 0.3 **b) Phase angle distribution for $\widetilde{\rho}$ = 0.3 and $\widetilde{U}$ = 3.5**

Fig. 7 Validation of decaying factor and phase-angle distribution with Huang's [30] results.

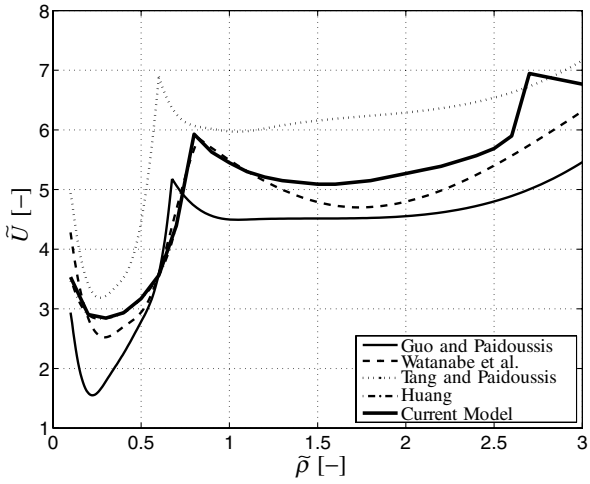

Fig. 8 Comparison of flutter boundary with results from literature [13,24,28,30].

Tanida [31], De Breuker et al. [7], and Tang and Païdoussis [23] have shown that the rigid part of the plate has a critical influence on the flutter speed. Here, a more detailed parametric study is conducted. The flutter speed is plotted against the mass ratio for various flexible part fractions f in Fig. 10. In this figure, the entire range of length ratios, from an almost fully rigid to a fully flexible plate, can be observed. Among the peculiarities of the flutter behavior of such partially rigid plate are the jumps in flutter speed with increasing mass ratio. These jumps are well known and described in literature as flutter mode jumps [13,14,26,28].

It can be seen from Fig. 10 that before the first jump, the flutter speed first decreases to a certain minimum, and increases again with increasing mass ratio. This trend occurs each time between two jumps. The mass ratios at which the jumps occur, called critical mass ratios, are dependent on the flexible part fraction f. They range from $\tilde{\rho} = 0.58$ to $\tilde{\rho} = 0.72$ for the first jump and from $\tilde{\rho} = 2.30$ to $\tilde{\rho} = 2.65$ for the second one, both for a flexible part fraction $f \in [0.2 \ldots 1.0]$. The gap between the second mode jump and the first mode jump is fairly large compared with the mass ratio of the first jump. This suggests that mode jump spacing becomes larger for higher modes. This is to be expected because mode spacing in the frequency domain increases for higher modes. It is also evident from Fig. 10 that the critical mass ratios decrease with decreasing value of f, and they are more sensitive to changes in values of f in the neighborhood of $f = 1.0$ than for smaller values.

The sensitivity of the flutter speed with respect to the flexible part fraction is illustrated in Fig. 11. It is observed that for lower mass ratios ($\tilde{\rho} \in [0.20 \ldots 0.50]$), the flutter speed increases with increasing value for f. This means that adding a rigid part to a flexible cantilever destabilizes the plate. For values larger than $\tilde{\rho} = 0.50$, the flutter speed mostly decreases with increasing f, meaning that the presence of a rigid part actually stabilizes the flexible plate. This stabilizing effect plays until the first jump. For mass ratios in between the two flutter mode jumps, the same phenomenon is present as previously described. We call the mass ratios at which the switch in the effect of the rigid part occurs as the crossover mass ratios. The first two of these are around $\tilde{\rho} = 0.50$ and $\tilde{\rho} = 1.50$.

The variation of the phase shift $\Delta\varphi$ between the upstream ($x = 0$) and downstream ($x = L$) part of the fluttering flexible part is shown for various mass ratios and length fractions in Fig. 12. As would be expected, jumps in the phase shift can be observed at exactly the same mass ratios of the jumps in flutter speed. In between the jumps,

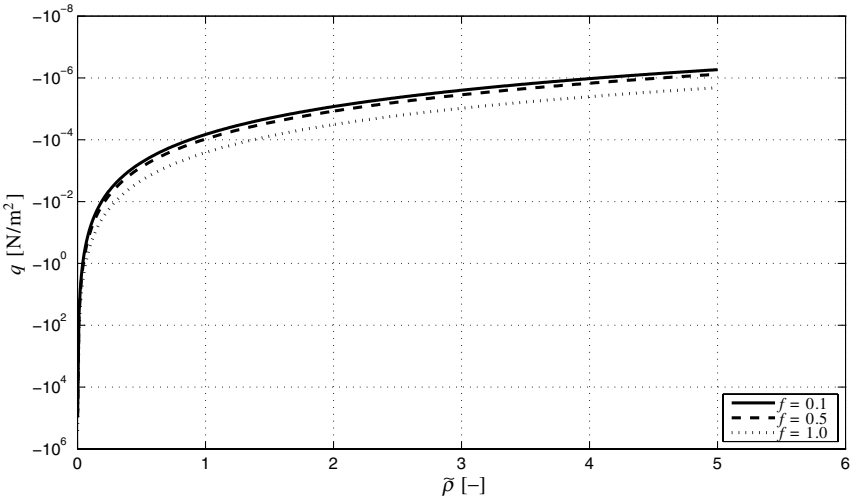

Fig. 9 Divergence speed eigenvalues.

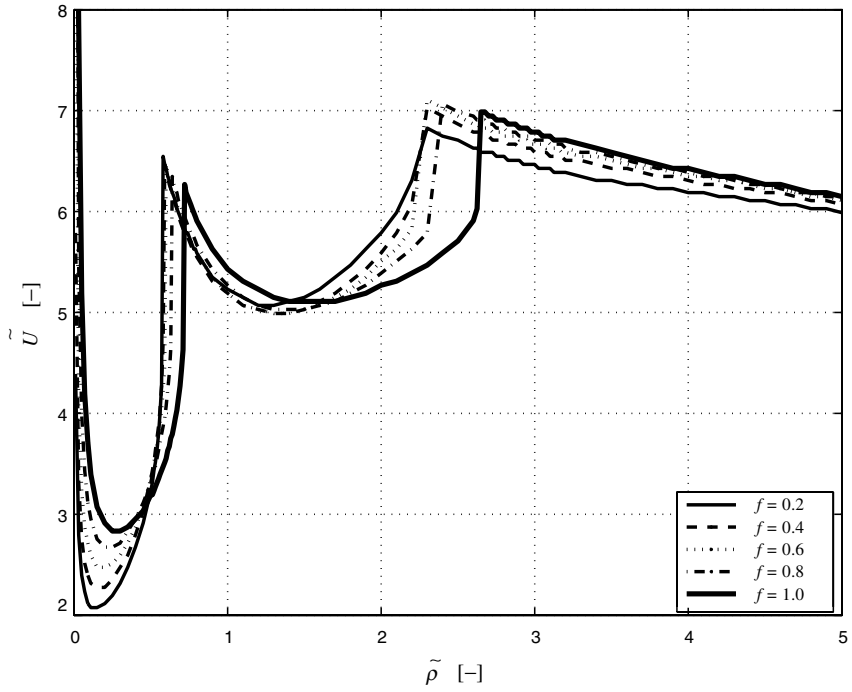

Fig. 10 Flutter speed vs mass ratio for various length fractions.

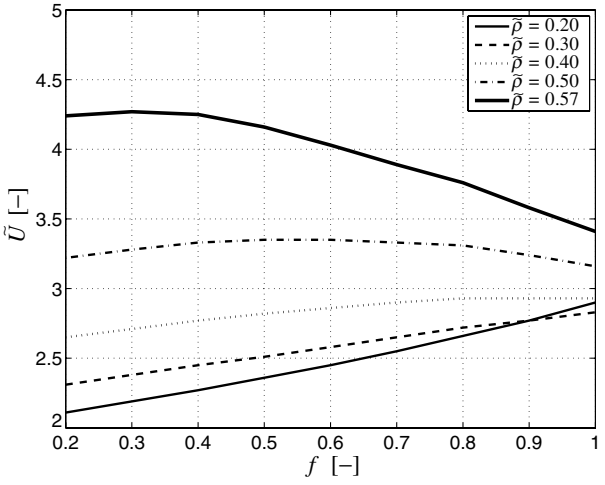

Fig. 11 Change in flutter speed with changing flexible to total length fraction f.

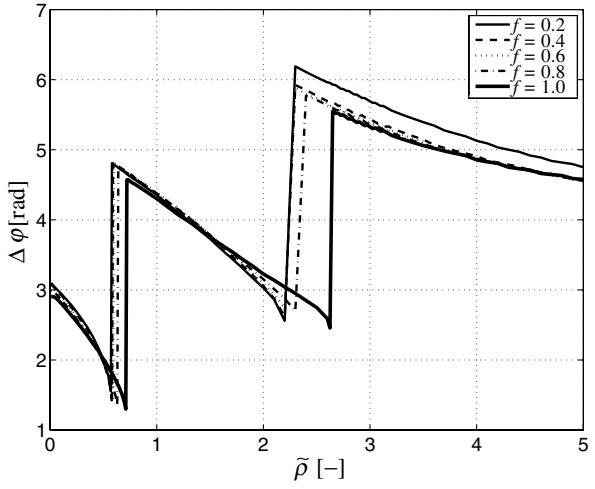

Fig. 12 Upstream–downstream edge phase shift vs mass ratio for various length fractions.

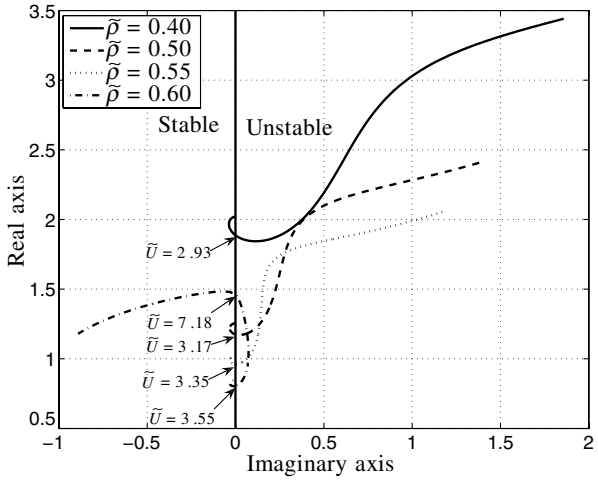

a) Second root locus branch for $f = 1.0$

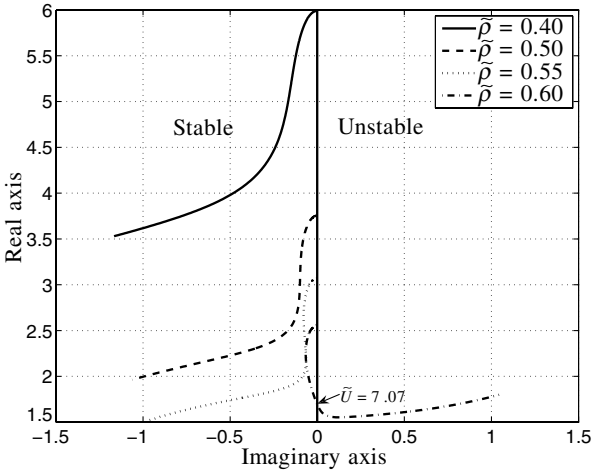

b) Third root locus branch for $f = 1.0$

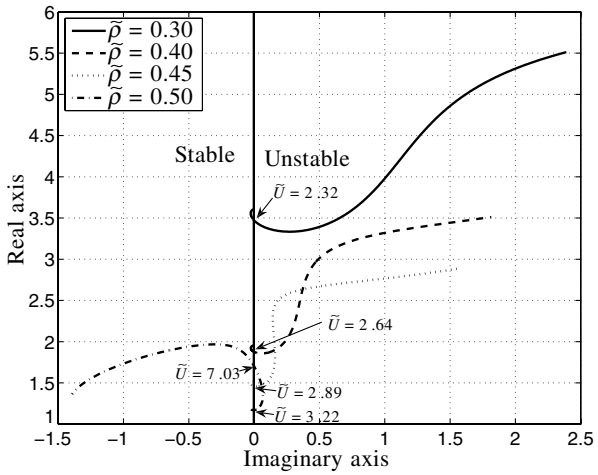

c) Second root locus branch for $f = 0.2$

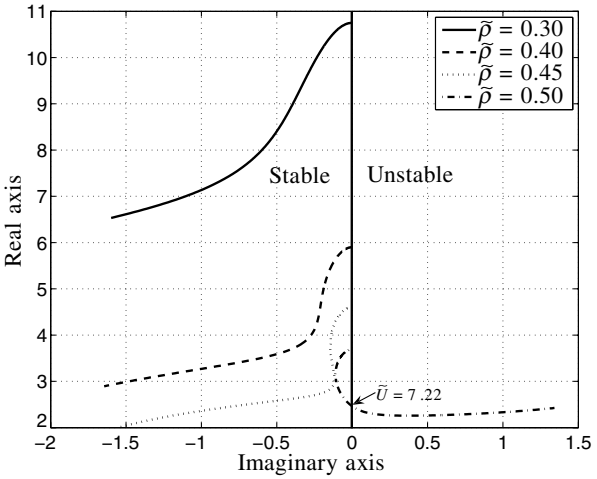

d) Third root locus branch for $f = 0.2$

Fig. 13 System root locus plots for a–b) $f = 1.0$ and c–d) $f = 0.2$.

the magnitude of the phase shift decreases with increasing mass ratio, which brings one to question the validity of Tanida's results [31], in which he assumes both the flutter mode shape and a constant phase difference.

Root locus plots, indicating how the eigenvalues of Eq. (29) change with flow velocity, are shown in Fig. 13 for two flexible part fractions ($f = 1.0$ and $f = 0.2$, respectively) and for selected mass ratios close to the first jump. When an ith branch is referred to, it means that it is the root locus branch that originates from the ith eigenfrequency of the system located on the imaginary axis. It is evident from Fig. 13a that for mass ratios $\tilde{\rho} \in [0.40 \ldots 0.55]$, the second branch goes into the unstable half of the complex plane, and subsequently is inclined to bend away hesitantly to the stable half again, but it continues into the unstable half plane. This phenomenon can be observed until a mass ratio of approximately 0.55. If $\tilde{\rho}$ is increased even further, the second branch returns, after going through the unstable half-plane, back to the stable half-plane. For most mass ratios, the third branch, depicted in Fig. 13b, is situated in the unstable half-plane when the second branch is in the stable half-plane and vice versa. However, for a certain range of mass ratios in the neighborhood of the flutter mode jumps at which, for a certain velocity range, both the second and third branches are in the stable half-plane. This means the system can have multiple critical points (i.e., multiple flow velocities at which a root locus branch crosses from the stable to the unstable half-plane), as also pointed out by Huang [30]. It is concluded from Figs. 13c and 13d that a change in length fraction only causes the previously described phenomenon to shift to lower mass ratios.

Figure 14 zooms into the root locus plots for mass ratios $\tilde{\rho} \in [0.55 \ldots 0.60]$ on the point where the second and third branches hesitate and turn back to the stable or unstable half-plane, respectively. It can be seen that the point at which both branches bend almost coincides at a value for $\tilde{U}$ of 7.20 for all mass ratios (see Fig. 14). This speed is a critical flow condition where the system becomes unstable. However, this speed is not shown on the flutter boundary of Fig. 10 because, at that point, the second branch still enters the unstable half-plane at a lower speed (see Figs. 13a and 13b). There, it is evident that at a mass ratio of 0.6 the branches switch. Also, the branch switching occurs at the same value for $\tilde{U}$ for every mass ratio. This interaction between modes is responsible [39] for the jumps in flutter mode engendering phenomena observed in Figs. 10 and 12. This issue also plays at the second jump. The fact that the two points, at which the branch bend, coincide almost has been observed earlier for pipes conveying fluids [17], though this is the first time it is also demonstrated for cantilevered plates in an axial flow and there are some clear and significant differences, in the sense that the second mode branches are crossing each other.

It is to be noted that for cases when the second branch returns to the stable half-plane after an excursion into the unstable half plane, the maximum negative damping ratio is relatively small in magnitude. So, although theoretically the plate would flutter in the second mode, in practice, the growth in amplitude of the oscillation in time would be small. Therefore, at mass ratios where the second branch bends back into the stable half-plane, the plate will probably be observed to flutter in the third mode, at a higher speed, and not in the second mode. Because of that, it might be efficacious to define the flutter

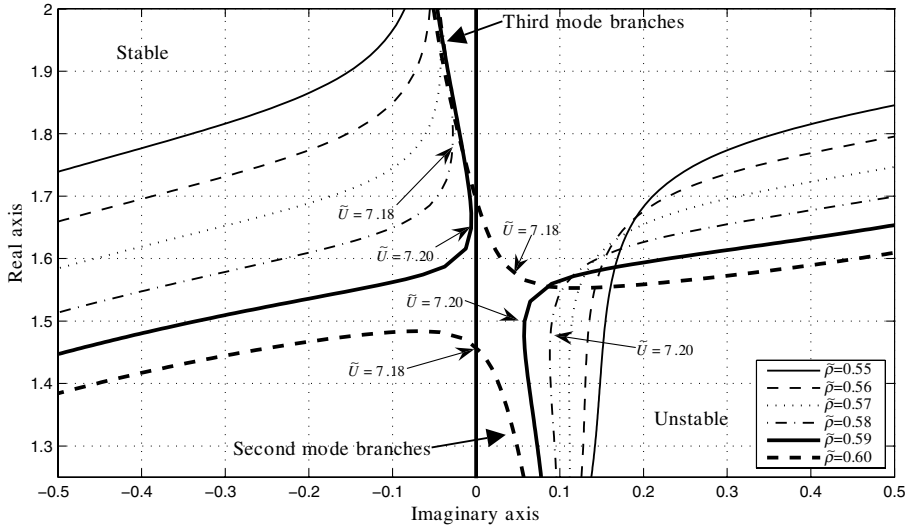

Fig. 14 Enlarged picture around the branch collision point.

boundary at values for the decay factor G larger than one instead of equal to one, as suggested already by Huang [30]. However, no well-motivated practical value for G was given by Huang. In the following, a suitably defined value for G is deduced that leads to a practical flutter boundary that better matches experimental results.

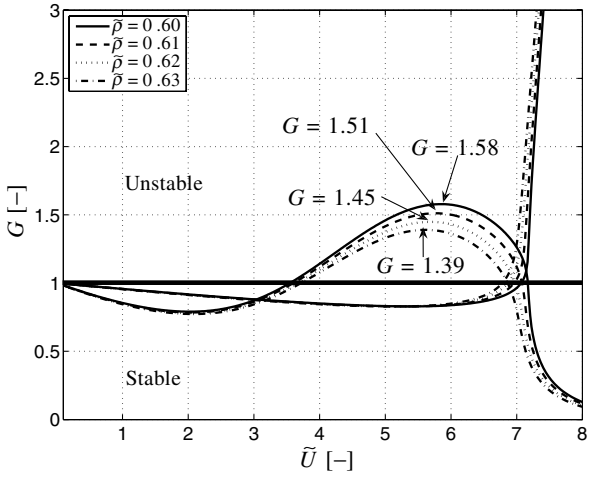

Fig. 15 Maximum values for the decay factor G for various mass ratios.

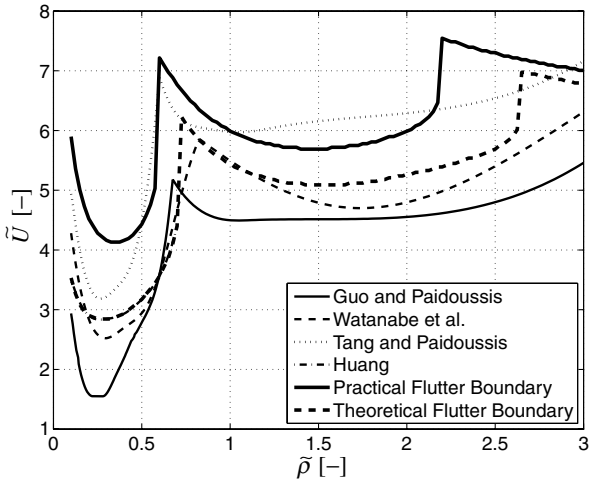

Fig. 16 Theoretical and practical flutter boundary, in comparison with results presented in literature [13,24,28,30].

Figure 15 shows the value for G of the second and third branch vs $\tilde{U}$ at mass ratios $\tilde{\rho} \in [0.60 \ldots 0.63]$. It is evident that the maximum value for G decreases with increasing mass ratio. These trends also play at lower values for f, obviously for lower mass ratios as can be derived from Fig. 11. For a wide range of $f \in [0.2 \ldots 1.0]$, the critical value for G remains approximately 1.60. If the excursion of the second branch in the unstable half plane is to be removed for these mass ratios, the boundary between the stable and unstable half-plane needs to be redefined as $G = 1.60$.

It is shown in Fig. 16 that the practical flutter boundary differs quantitatively, not qualitatively, from the one shown in Fig. 10. It can be seen that the flutter speed is higher and the jumps occur at lower mass ratios. If the practical flutter boundary is compared with the results from literature [13,24,28,30], it is clear from Fig. 16 that this flutter boundary is shifted much closer to the results obtained by Tang and Païdoussis [23,24], both in terms of magnitude of the flutter speed, and location of the first jump in flutter speed. Tang and Païdoussis [23,24] have demonstrated to match experimental results better than existing theories. They model the aeroelastic cantilevered plate problem using an inextensible beam model and a lumped vortex element aerodynamic model, integrated in time. The fact that the proposed practical flutter boundary matches the latter results better might reveal part of the mystery plaguing the problem of cantilevered plate flutter. Several experimental results [25,29] have shown that the flutter phenomenon is subcritical, while all theories [23] predict supercritical bifurcation. It might be the case that although actual flutter is observed in a certain mode, another mode becomes unstable earlier but for a limited speed range. The latter might then be observed as a subcritical oscillation. This statement is illustrated by considering Fig. 13 where, for instance, at a mass ratio of 0.6, the third branch becomes unstable, whereas the second branch only shows a little excursion in the unstable half of the plane and then returns to the stable half again. This part of the branch in the unstable half-plane can hence be responsible for the subcritical vibrations. Obviously, this effect does not play in the lower mass ratio range. However, Tang et al. [25] also observed experimentally subcritical bifurcation at mass ratios around 0.05. Therefore, the proposed mechanism does not fully explain this phenomenon, but points out a possibility which needs to be investigated further.

VIII. Conclusions

Analysis of partially rigid cantilevered two-dimensional plates is carried out in the Laplace domain using the Rayleigh–Ritz approach. Results are validated against published results in literature and found to be in good agreement with those published results. The behavior of the plate is described by three nondimensional parameters, the mass ratio $\tilde{\rho}$, the flexible part fraction f of the flexible part to the total

length, and the nondimensional speed $\tilde{U}$. The flutter boundary in the $\tilde{\rho}$-$\tilde{U}$ graph shows that jumps in flutter speed occur for certain values of the mass ratio. The flexible part fraction f alters the flutter boundary quantitatively, though not qualitatively. There exist ranges of mass ratios for which the presence of a rigid part destabilizes the flexible plate, and mass ratios at which the rigid part stabilizes the plate. The phase-angle difference between the upstream and downstream part of the flexible plate shows the same behavior as the flutter speed with changing mass ratio. In particular, the phase shift is not constant with changing mass ratio.

The jump in flutter mode is studied by investigating the root locus branches of the aeroelastic system. The reason for the jumps is found to be caused by a collision of flutter mode branches in the root locus plane.

Acknowledgments

The micro aerial vehicle wing concept investigated in this paper was developed by the first author in collaboration with Roelof Vos as a part of their respective Master of Science work at the Delft University of Technology under the supervision of Zafer Gürdal and Michel Van Tooren, respectively. The authors wish to warmly acknowledge the contribution of Michel Van Tooren and Roelof Vos to the development of the project. The authors would also like to thank Ron Barrett. His remarks regarding possible aeroelastic instability of the wing concept provided the incentive for the research presented in this paper. The authors would like to thank the rest of the members of the project, Lars Krakers and Domenico Casella. Special thanks go to Lixi Huang for his valuable comments in the phase angle distribution.

References

[1] Kudva, J., "Overview of the DARPA Smart Wing Project," *Journal of Intelligent Material Systems and Structures*, Vol. 15, April 2004, pp. 261–267. doi:10.1177/1045389X04042796

[2] Gano, S., and Renaud, J., "Optimized Unmanned Aerial Vehicle with Wing Morphing for Extended Range and Endurance," *9th AIAA/ISSMO Symposium and Exhibit on Multidisciplinary Analysis and Optimization*, AIAA Paper 2002-5668, 2002.

[3] Joshi, S., Tidwell, Z., Crossley, W., and Ramakrishnan, S., "Comparison of Morphing Wing Strategies Based upon Aircraft Performance Impacts," *Proceedings of the 45th AIAA/ASME/ASCE/AHS/ASC Structures, Structural Dynamics, and Materials Conference*, AIAA Paper 2004-1722, 2004.

[4] De Breuker, R., "Structural and Aeroelastic Modelling of Adaptive Beams," M.S. Thesis, Delft Univ. of Technology, Delft, The Netherlands, Dec. 2004.

[5] Vos, R., De Breuker, R., Barrett, R., and Tiso, P., "Morphing Wing Flight Control via Post-Buckled Precompressed Piezoelectric Actuators," *Journal of Aircraft*, Vol. 44, No. 4, July–Aug. 2007, pp. 1060–1068. doi:10.2514/1.21292

[6] De Breuker, R., Tiso, P., Vos, R., and Barrett, R., "Nonlinear Semi-Analytical Modeling of Post-Buckled Precompressed (PBP) Piezoelectric Actuators for UAV Flight Control," *Proceedings of the 48th AIAA/ASME/ASCE/AHS/ASC Structures, Structural Dynamics, and Materials Conference*, AIAA Paper 2006-1795, 2006.

[7] De Breuker, R., Abdalla, M., and Gürdal, Z., "Flutter of Partially Rigid Cantilevered Plates in Axial Flow," *Proceedings of the 48th AIAA/ASME/ASCE/AHS/ASC Structures, Structural Dynamics, and Materials Conference*, AIAA Paper 2006-1730, 2006.

[8] "Smart Structures and Materials, 2006: Smart Structures and Integrated Systems," *Proceedings of the SPIE*, Vol. 6173, Edited by Matsuzaki, Yuji, 2006, pp. 121–132.

[9] Dowell, E., "Nonlinear Oscillations of a Fluttering Plate," *AIAA Journal*, Vol. 4, No. 7, July 1966, pp. 1267–1275.

[10] Dowell, E., "Flutter of Infinitely Long Plates and Shells, Part 1: Plate," *AIAA Journal*, Vol. 4, No. 8, Aug. 1966, pp. 1370–1377.

[11] Dowell, E., *Aeroelasticity of Plates and Shells*, Noordhoff International, Leyden, The Netherlands, 1975.

[12] Kornecki, A., Dowell, E., and O'Brien, J., "On the Aeroelastic Instability of Two-Dimensional Panels in Uniform Incompressible Flow," *Journal of Sound and Vibration*, Vol. 47, No. 2, 1976, pp. 163–178. doi:10.1016/0022-460X(76)90715-X

[13] Guo, C., and Païdoussis, M., "Stability of Rectangular Plates with Free Side-Edges in Two-Dimensional Channel Flow," *Journal of Applied Mechanics*, Vol. 67, No. 1, 2000, pp. 171–176. doi:10.1115/1.321143

[14] Païdoussis, M., *Fluid-Structure Interactions: Slender Structures and Axial Flow*, Vol. 2, Elsevier, Amsterdam, 2004.

[15] Gregory, R., and Païdoussis, M., "Unstable Oscillation of Tubular Cantilevers Conveying Fluid, 1: Theory," *Proceedings of the Royal Society A: Mathematical, Physical and Engineering Sciences*, Vol. 293, No. 1435, 1966, pp. 512–527. doi:10.1098/rspa.1966.0187

[16] Païdoussis, M., *Fluid-Structure Interactions: Slender Structures and Axial Flow*, Vol. 1, Academic Press, New York, 1998.

[17] Ryu, S., Sugiyama, Y., and Ryu, B., "Eigenvalue Branches and Modes for Flutter of Cantilevered Pipes Conveying Fluid," *Computers and Structures*, Vol. 80, Nos. 14–15, 2002, pp. 1231–1241. doi:10.1016/S0045-7949(02)00083-4

[18] Païdoussis, M., Sarkar, A., and Semler, C., "Horizontal Fluid-Conveying Cantilever: Spatial Coherent Structures, Beam Modes and Jumps in Stability Diagram," *Journal of Sound and Vibration*, Vol. 280, Nos. 1–2, 2005, pp. 141–157. doi:10.1016/j.jsv.2003.12.026

[19] Shayo, L., "Stability of Cantilever Plates in Uniform Incompressible Flow," *Journal of Sound and Vibration*, Vol. 68, No. 3, Feb. 1980, pp. 341–350. doi:10.1016/0022-460X(80)90391-0

[20] Weiliang, Y., and Dowell, E., "Limit Cycle Oscillations of a Fluttering Cantilever Plate," *AIAA Journal*, Vol. 29, No. 11, Nov. 1991, pp. 1929–1936.

[21] Tang, D., and Dowell, E., "Limit Cycle Oscillations of Two-Dimensional Panels in Low Subsonic Flow," *International Journal of Non-Linear Mechanics*, Vol. 37, No. 7, Oct. 2002, pp. 1199–1209. doi:10.1016/S0020-7462(01)00140-8

[22] Attar, P., Dowell, E., and Tang, D., "Modeling Aerodynamic Nonlinearities for Two Aeroelastic Configurations: Delta Wing and Flapping Flag," *Proceedings of the 44th AIAA/ASME/ASCE/AHS Structures, Structural Dynamics, and Materials Conference*, AIAA Paper 2003-1402, 2003.

[23] Tang, L., and Païdoussis, M., "On the Instability and the Post-Critical Behaviour of Two-Dimensional Cantilevered Flexible Plates in Axial Flow," *Journal of Sound and Vibration*, Vol. 305, Nos. 1–2, 2007, pp. 97–115. doi:10.1016/j.jsv.2007.03.042

[24] Tang, L., and Païdoussis, M., "Influence of the Wake on the Stability of Cantilevered Flexible Plates in Axial Flow," *Journal of Sound and Vibration*, Vol. 310, No. 3, Feb. 2008, pp. 512–526.

[25] Tang, D., Yamamoto, H., and Dowell, E., "Flutter and Limit Cycle Oscillations of Two-Dimensional Panels in Three-Dimensional Axial Flow," *Journal of Fluids and Structures*, Vol. 17, No. 2, 2003, pp. 225–242. doi:10.1016/S0889-9746(02)00121-4

[26] Watanabe, Y., Isogai, K., Suzuki, S., and Sugihara, M., "Theoretical Study of Paper Flutter," *Journal of Fluids and Structures*, Vol. 16, No. 4, 2002, pp. 543–560. doi:10.1006/jfls.2001.0436

[27] Balint, T., and Lucey, A., "Instability of a Cantilevered Flexible Plate in Viscous Channel Flow," *Journal of Fluids and Structures*, Vol. 20, No. 7, Oct. 2005, pp. 893–912. doi:10.1016/j.jfluidstructs.2005.05.005

[28] Yadykin, Y., Tenetov, V., and Levin, D., "Flow-Induced Vibration of a Flexible Strip Hanging Vertically in a Parallel Flow, Part 1: Temporal Aeroelastic Instability," *Journal of Fluids and Structures*, Vol. 15, No. 8, Nov. 2001, pp. 1167–1185. doi:10.1006/jfls.2001.0400

[29] Watanabe, Y., Suzuki, S., Sugihara, M., and Sueoka, Y., "Experimental Study of Paper Flutter," *Journal of Fluids and Structures*, Vol. 16, No. 4, 2002, pp. 529–542. doi:10.1006/jfls.2001.0435

[30] Huang, L., "Flutter of Cantilevered Plates in Axial Flow," *Journal of Fluids and Structures*, Vol. 9, No. 2, Feb. 1995, pp. 127–147. doi:10.1006/jfls.1995.1007

[31] Tanida, Y., "Stability of a Soft Plate in Channel Flow," *JSME International Journal, Series B (Fluids and Thermal Engineering)*, Vol. 44, No. 1, 2001, pp. 8–13. doi:10.1299/jsmeb.44.8

[32] Argentina, M., and Mahadevan, L., "Fluid-Flow-Induced Flutter of a Flag," *Proceedings of the National Academy of Sciences of the United*

States of America, Vol. 102, No. 6, 2005, pp. 1829–1834. doi:10.1073/pnas.0408383102

[33] Brush, B., and Almroth, D., *Buckling of Bars, Plates, and Shells*, McGraw–Hill, New York, 1975.

[34] Theodorsen, T., "General Theory of Aerodynamic Instability and the Mechanism of Flutter," NASA TR 496, 1935.

[35] Schmidt, E., "Zur Theorie der Linearen und Nichtlinearen Integralgleichungen, 1 Teil: Entwicklung Willkürlicher Funktionen nach Systemen Vorgeschriebener," *Mathematische Annalen*, Vol. 63, No. 4, March 1907, http://gdz.sub.uni-goettingen.de.

[36] Anderson, J., *Fundamentals of Aerodynamics*, 2nd ed., McGraw–Hill, New York, 1991.

[37] Mesaric, M., and Kosel, F., "Unsteady Airload of an Airfoil with Variable Camber," *Aerospace Science and Technology*, Vol. 8, No. 3, April 2004, pp. 167–174. doi:10.1016/j.ast.2003.10.007

[38] Glauert, H., *Elements of Aerofoil and Airscrew Theory*, Cambridge Univ. Press, Cambridge, England, U.K., 1948.

[39] Seyranyan, A., "Collision of Eigenvalues in Linear Oscillatory Systems," *Journal of Applied Mathematics and Mechanics*, Vol. 58, No. 5, 1994, pp. 805–813. doi:10.1016/0021-8928(94)90005-1

E. Livne
Associate Editor